Journal of Ship Production and Design, Vol. 36, No. 4, November 2020, pp. 271–279
http://dx.doi.org/10.5957/JSPD.07190033

A Three-Dimensional Model for Strength Assessment of Type-C Independent Cargo Tank Structures

Ming Song,* Bin Qin,† Li Zhou,* and **Zhengru Ren‡**

*School of Naval Architecture and Ocean Engineering, Jiangsu University of Science and Technology, Zhenjiang, China
†Jiangnan Shipyard (Group) Co., Ltd., Shanghai, China
‡Marine Technology, Norwegian University of Science and Technology, Trondheim, Norway

For the analysis of the arrangement and strength of Type-C independent cargo tank structures, the linear spring or rod elements are usually used to model supporting woods, in which one-dimensional and linear contact behaviors are assumed. This study aimed at developing a three-dimensional model for achieving more accurate strength assessment. In the model, solid elements are modeled to simulate the supporting woods. The nonlinear contact between the cargo tanks and the supporting woods is taken into account through LS-DYNA software. Numerical simulations of a 22,000-m^3 liquefied petroleum gas carrier are carried out using both one-dimensional and three-dimensional models. Three load cases including one static and two dynamic cases are considered to assess the strength of the tank structures and supporting woods. The results obtained by the proposed model are compared with the results on the basis of spring elements. It is found that this new model can provide more reasonable strength predictions of the tank structures and the supporting woods. The method based on spring elements underestimates the wood stress, which indicates that it may be not conservative. Some discussions and suggestions are presented.

Keywords: strength assessment; spring elements; supporting wood; three-dimensional model; type-C independent cargo tank

1. Introduction

The rise of global energy demand is a result of a growth in the world's population. Many researchers forecast that by 2050, there could be 2.5 billion more humans than today, who would use twice the energy consumed today (Thiagarajan & Seah 2016). To fulfill the energy requirement, all possible sources of energy are being examined. Natural gas is an abundant clean and efficient energy resource that is still relatively a newer source for exploitation. With the advance of technology, natural gas can be an alternative fuel to generate electricity and the operating costs are comparable to coal or nuclear energy sources. Besides, liquefied petroleum gas (LPG) is a clean-burning fossil fuel that can be used for various heating purposes and in internal combustion engines. It is a by-product from crude oil refining and natural gas processing. Although petroleum gas is a relatively small energy source, more than 240 million tons are consumed worldwide each year (The world LP Gas Association 2010).

With an increasing demand for cleaner fuels, both natural and petroleum gas transport are growing. Because of long-distance marine transportation and economic issues, both natural and petroleum gases are pressurized, cooled, and transported in liquefied state, by means of special ships called liquefied gas carriers. Innovative technical achievements have improved the compactivity of clean energy (Blanc et al. 2004; Remeljej & Hoadley 2006; Morosuk et al. 2012; Lim et al. 2013; Lee et al. 2015). Depending on the cargo type, liquefied natural gas (LNG) and LPG are distinguished.

For liquefied gas transport, different cargo tanks are used: integral tanks, membrane tanks, semi-membrane tanks, and independent tanks. Independent cargo tanks are self-supported structures and do

Manuscript received by JSPD Committee May 30, 2020; accepted June 25, 2020.
Corresponding author: Ming Song, songmingcssc@163.com

not contribute to the strength of the hull. This category can be further subdivided into types A, B, and C (IMO 2014). Type-A tanks are designed according to recognized standards or class rules and require a full secondary barrier. Type-B tanks are designed using model tests and refined analysis methods and only require a partial secondary barrier. Both Type-A and Type-B tanks have a design vapor pressure of less than .7 bar. By contrast, Type-C tanks are generally pressure vessels which require no additional secondary barriers (Thiagarajan & Seah 2016). Because of its safety, reliable design, and good operational records, the Type-C independent cargo tank occupies a considerable proportion in the small- and medium-sized liquefied gas ship market. Ships with independent Type-C tank are applicable for carrying a wide range of liquefied gases, such as LPG, LNG, and ethylene. Lately, there has been an increased demand for small LNG carriers for coastal service where the Type-C independent tank has shown to be competitive and flexible for the operators.

The Type-C independent cargo tank requires a high-level structural safety performance, as the transport of gas is hazardous because of potential dangers such as fire, toxicity, corrosiveness reactivity, low temperature, and high pressure (Senjanović et al. 2006). A traditional Type-C independent cargo tank consists of a cylindrical midbody with hemispherical, elliptical, or torispherical end caps supported by two saddles. Laminated wood is laid between the tank and supporting saddles and subjected to a mechanical load from the cargo tank. It is necessary to confirm the adequacy of the arrangement and strength of tank structures and supporting wood with the specified loading conditions in accordance with relevant rules and regulations, e.g., the International Code for Construction and Equipment of Ships Carrying Liquefied Gases in Bulk (IGC Code). The Unified Requirements G1 and G2 of the IGC Code are specified by the International Association of Classification Societies (IACS), and each of the IACS members has incorporated this document into their own classification rules. According to the classification rules (ABS 2010; BV 2012; DNV 2013a; LR 2016), finite element analysis should be carried out to evaluate the stress levels of structures and supporting wood. The strength of the tank structures and the hull structures can be analyzed independently (DNV 2013b), and the linear spring or rod elements can be used to model the supporting chocks (ABS 2010; BV 2012). However, there are several limitations of the assumption of spring or rod elements. The spring or rod elements are acting as containing compressive force in the radial direction, which means that the contact between the tank shell and supports is only considered in one dimension. The effects of the nonlinear contact relationship between the tank shell and the supporting wood is neglected. Because cargo tank supporting chocks do not physically carry any tensional forces, the final results are to be obtained by progressively removing those rod elements that are in tension. In some cases, it may take several iterations to reach the final force equilibrium. The nonlinear GAP elements are proposed for modeling the supporting chocks in the LR rules (2016), in which the analysis will be nonlinear and automatically iterate until the solution converges. Initial gap and preload can be taken as zero unless specified by the designer. However, the mentioned methods are not able to reflect the real contact characteristics as one-dimensional contact behavior is assumed, which may result in low precision of strength estimation for both tank structures and supporting wood.

The study presented in this article is motivated by the limitations of published methods for strength assessment of the Type-C independent cargo tank structure. This study aimed at developing a three-dimensional model to assess the structural strength by using a nonlinear finite element analysis method. In this three-dimensional model, the supporting woods are modeled using solid elements and the nonlinear contact between the tank and the supporting woods is simulated. The three-dimensional model is applied to a case study where a 22,000-m^3 LPG carrier with four independent tanks is analyzed. Three load cases including one static and two dynamic cases are taken into account. These numerical simulations are performed by LS-DYNA software (Hallquist 2013). In addition, the one-dimensional model where the linear spring elements represent the supporting woods is also used to assess the structural strength by Patran software. The results of the two models, including the maximum stresses of the tank structures and the supporting wood, are compared and discussed. The main findings from the comparison are highlighted in this article.

The article is organized as follows: Sections 2 and 3 describe the characteristics of the support structure of the Type-C independent cargo tank and the detailed calculation of design loads, respectively. Section 4 presents the details of the one-dimensional and three-dimensional models. Section 5 presents a case study of a 22,000-m^3 LPG carrier and a comparison of the results obtained using the both models, and the conclusions are given in Section 6.

2. Support structure description

A ship with independent Type-C tanks is composed of a main hull frame, supporting saddles, and a liquid cargo tank. A traditional Type-C independent cargo tank consists of a cylindrical midbody with hemispherical, elliptical, or torispherical end caps. Each tank is supported by two saddles. Considering the effects of thermal expansion and cold contraction, the saddles are set as a fixed saddle and a sliding saddle. The saddle and the tank body are connected by laminated wood which do not physically carry any tensional forces. The upper and lower surfaces of the laminated wood are, respectively, fixed on the saddle panel and the cylinder steel plate with epoxy cement. The typical support structure of a Type-C independent cargo tank is shown in Fig. 1, including fixed 1) and sliding 2) supporting chocks.

3. Design loads

The design loads are to be considered for strength evaluation of the Type-C independent cargo tank. According to the IGC Code, the design shall take into account proper combinations of the following loads: internal pressure, external pressure, dynamic loads due to the ship motion, thermal loads, and so on. For the details, please refer to the IGC Code. The internal vapor pressure and the cargo tank pressure which are applied in our study are described in the following sections.

3.1. Internal vapor pressure

The design vapor pressure should not be less than the maximum design vapor pressure p_0 in MPa, as given by the following equations:

$$p_0 = 0.2 + AC(\rho_r)^{1.5} \text{ and} \quad (1)$$

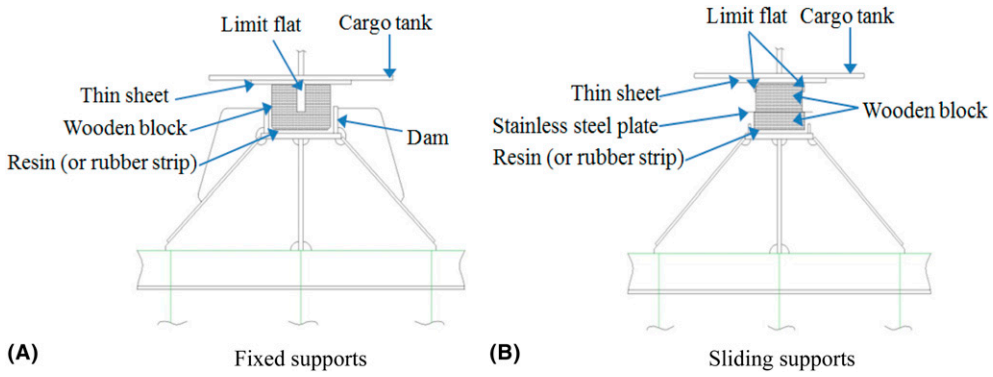

Fig. 1 Typical support structure of Type-C independent cargo tank

$$A = 0.00185([\sigma_m/\Delta\sigma_A])^2, \tag{2}$$

where ρ_r is the relative density of the cargo ($\rho_r = 1$ for fresh water) at the design temperature, σ_m is the design primary membrane stress, $\Delta\sigma_A$ is the allowable dynamic membrane stress, and $C = \max\{h, 0.75b, 0.45l\}$ is a characteristic tank dimension, where h, b, and l are the height, width, and length of the tank, respectively.

3.2. Cargo tank pressure

The internal liquid pressures are created by the resulting acceleration of the cargo center of gravity due to the ship motions. The design cargo tank pressure at a given location in the tank is calculated as follows:

$$p_{eq} = p_0 + (p_{gd})_{max} \tag{3}$$

$$(p_{gd})_{max} = \frac{\rho_C \times \alpha_\beta \times Z_\beta}{102,000}, \tag{4}$$

where p_0 is the design vapor pressure; $(p_{gd})_{max}$ is the maximum combined internal liquid pressure in MPa, resulting from the combined effects of gravity and dynamic acceleration; ρ_C is the maximum density of the cargo at the design temperature; α_β is the dimensionless acceleration relative to the gravitational acceleration, resulting from gravitational and dynamic loads, in an arbitrary direction β (see Fig. 2); Z_β is the largest liquid height above the point where the pressure can be determined from the tank shell in the β direction (see Fig. 3); and β is the angle of the acceleration vector relative to the vertical plan at a given point on the ellipsoid in the transverse direction (Y–Z plane). For large tanks, an acceleration ellipsoid taking account of transverse vertical and longitudinal accelerations should be used. The unit of p_{eq} and $(p_{gd})_{max}$ is MPa.

4. One-dimensional and three-dimensional models

4.1. One-dimensional model

In the traditional way, the wood blocks between the cargo tank and the support structures are usually simulated as spring elements with the length of the elements similar to its thickness. A cylindrical coordinate system is built at the axis of the tank cylindrical shell with U_R, U_T, and U_Z in the radial, circumferential, and axial directions, respectively. The spring elements are all modeled in the radial direction connected to the tank shell. The stiffness of the springs K is given by the following equation:

$$\frac{1}{K} = \frac{H}{A_1 E_{\|}}, \tag{5}$$

where H is the thickness of the laminated wood block, A_1 is the contact area between one wood block and tank, and $E_{\|}$ is the elastic modulus of the wood.

Commercial software MSC Patran/Nastran can be applied. The spring elements representing the support woods can be disconnected when they are in tension, i.e., no contact. Thus, a manual iterative procedure is required. In each step of the iteration, spring elements which are in tension are removed and the FE model rerun

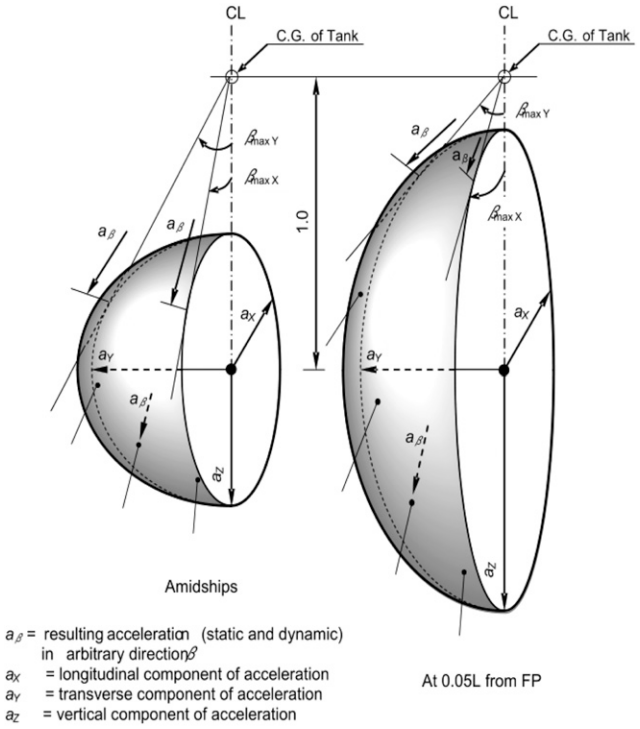

Fig. 2 Acceleration ellipsoid (refer to IMO 2014)

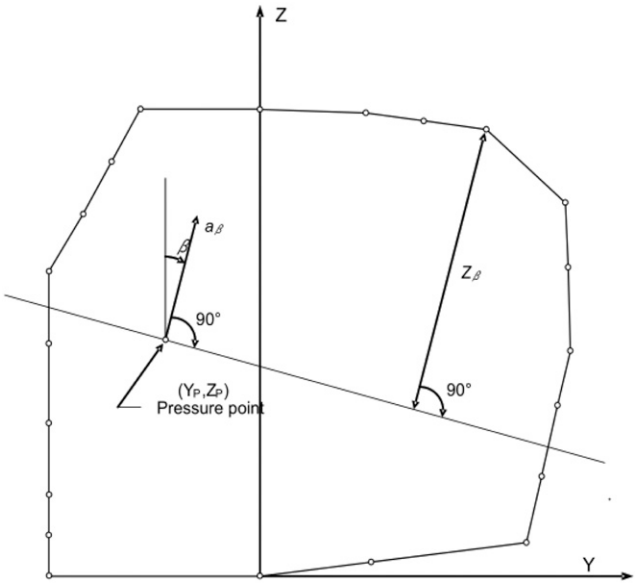

Fig. 3 Liquid height (refer to IMO 2014)

until all active supports are in compression. To detect and remove the spring elements in tension automatically, a subroutine is developed to incorporate into the Nastran solver.

All boundary constraints are based on the cylindrical coordinate system created as mentioned previously. The cradles of the tank are regarded as rigid foundation with no deformation at the lower surface of the laminated wood. Therefore, the spring elements connected to the fixed and sliding supports are constrained in the radial direction and circumferential direction as $U_R = U_T = 0$. The longitudinal displacement of the cargo tanks is restrained at a fixed support, and $U_Z = 0$ is applied to all upper and lower nodes of the spring elements of the fixed saddles.

4.2. Three-dimensional model

To achieve more accurate strength assessment, a three-dimensional model is proposed. The numerical simulations are performed with nonlinear explicit FEM software LS-DYNA. The supporting wood blocks are modeled using eight-node solid elements with reduced integration, in which three-dimensional contact between the tank shell and supports is taken into account. To ensure the accuracy of the numerical results, the mesh size for the wood is the same as the mesh size of tank structures around the contact area. LS-DYNA has a material (MAT_WOOD, Material Type 143) that can be used for the wood.

In LS-DYNA, the command of CONTACT provides a way of treating interaction between disjoint parts. The contact between the tank outer shell and the upper surfaces of fixed and sliding supporting wood is implemented using a contact-automatic surface-to-surface formulation with a static coefficient of friction of .45. As this contact type has no orientation and always considers shell thickness, it is necessary that the shell and wood surfaces are modeled with at least a small gap between them. To avoid initial penetrations, the gap between the tank and the wood should be no less than half the thickness of the tank shell potentially in contact. The contact between the two components of sliding supports is also implemented using the contact-automatic surface-to-surface formulation with a dynamic coefficient of friction of .2 (DNV 2013b). No gap is necessary between solid elements.

The combined hydrostatic and hydrodynamic pressure p_{eq} is applied on the element through the command of LOAD_SEGMENT_SET with DEFINE_FUNCTION. The constraint is implemented on nodes at the lower surface of the wood using BOUNDARY_SPC_SET, in which the boundary conditions are the same as those in the one-dimensional model.

5. Case study

A 22,000-m^3 LPG carrier with four independent tanks is analyzed in this study. The main dimensions are listed in Table 1. Cargo tanks labeled with No. 2 to No. 4 share a similar design. The No. 4 tank is selected as the research target as it is the tank with the severest condition. Both one-dimensional and three-dimensional models are used here to assess the structural strength.

5.1. Finite element model

The one-dimensional model is shown in Fig. 4, in which the yellow lines are spring elements representing the supporting wood. The three-dimensional model is shown in Fig. 5, in which the yellow part and the red part represent the fixed wood and the sliding wood, respectively. All tank structures are modeled as shell elements. According to the China Classification Society (CCS) rules (2016), a coarse mesh size for shell elements should be $R/30$, where R is the radius of the cargo tank (see Table 1). Thus, a coarse mesh

Table 1 Principal particulars

Length of B.P.	153.00 m
Length of scantling	151.49 m
Breadth	25.40 m
Depth	16.70 m
Design draft	8.50 m
Scantling draft	11.20 m
Number of cargo tanks	4
Radius of cargo tank	11.3 m

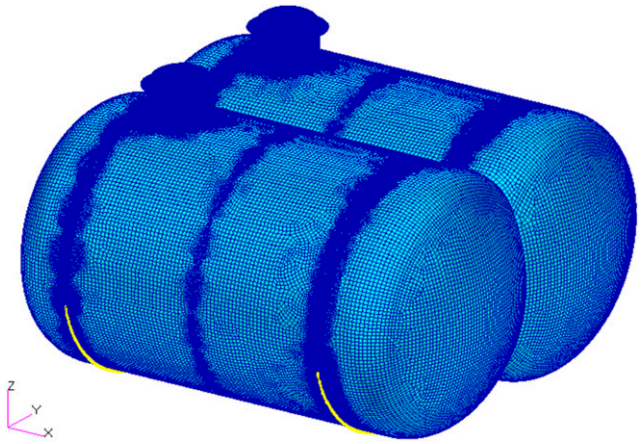

Fig. 4 One-dimensional model; the yellow lines are spring elements

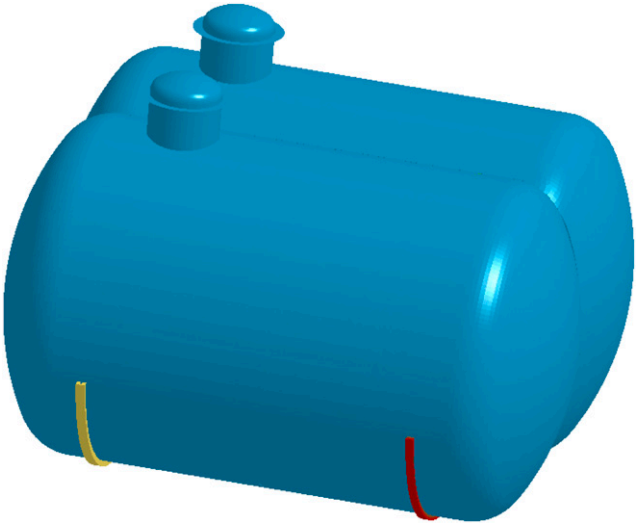

Fig. 5 Three-dimensional model; the yellow and red parts are solid elements

with an element size not larger than 250 mm × 250 mm is applied for general parts and a fine mesh with an element size less than 50 mm × 50 mm for critical areas in the finite element model. The elastic material model is used for the tank structure: Young's Modulus is 2.06 E+5 N/mm^2, Poisson's ratio is .3, density is 7.85 E−9 t/mm^3, yield stress is 355 N/mm^2, and tensile strength is 490 N/mm^2. The wood material parameters are Young's modulus (parallel to layer) is 1.19 E+4 N/mm^2, Poisson's ratio is .3, density is 1.35 E−9 t/mm^3, and compressive strength (perpendicular to layer) is 240 N/mm^2.

5.2. Design load case

One static and two dynamic load cases are selected to assess the strength of the cargo tank structures and the supporting wood blocks. The maximum design vapor pressure p_0 is .53 MPa, which is applied on tank shell structures in all load cases. According to the IGC Code, a static angle of heel of 30° with tank dead weight gravity should be considered for the static load case and combination of gravity and dynamic accelerations for dynamic load cases. The details of the load cases are defined in Table 2, and all parameters are referring to the IGC Code.

For the static load case, liquefied cargo pressure without acceleration and inertial load of g are applied on the tank structure in the angle of 30°. For the dynamic load case, acceleration in the Y–Z plan is considered, whereas it is neglected in the longitudinal direction. Combined acceleration angles of 0° and 10° are considered to verify the governing condition in dynamic loads. The combined hydrostatic and hydrodynamic pressure p_{eq} based on equation (4) is applied on the tank structure in all load cases. Figure 6 shows combined hydrostatic pressure for load case 1.

Table 2 Static and dynamic load cases

Load case		Acceleration angle β	Combined acceleration α_β/g
Static	LC1	30°	1.00
Dynamic	LC2	0°	1.57
	LC3	10°	1.53

g, acceleration of gravity.

5.3. Comparisons and discussions

Both one-dimensional and three-dimensional models are used to assess the strength of the tank structures and the supporting woods for the three load cases. The comparisons of results obtained by the two models are carried out.

5.3.1. Comparison of maximum stress. The maximum stresses of the tank structures and the supporting woods obtained by both one-dimensional and three-dimensional models are presented in Tables 3–5. The discrepancy defined as $(S_1 - S_3)/S_1$ is also given in the tables.

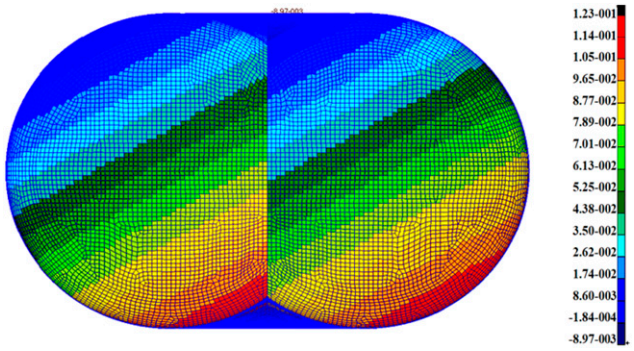

Fig. 6 Combined hydrostatic pressure plotted on the FE-model of No. 4 tank

Table 3 Comparison of results for load case 1

Component	One-dimensional model S_1 (MPa)	Three-dimensional model S_3 (MPa)	Discrepancy $\frac{S_1-S_3}{S_1}$ (%)
Tank shell	360	335	7
Dome shell	495	494	0
Tank longitudinal bulkhead	268	215	20
Tank support rings	249	146	41
Tank vacuum rings	368	346	6
Fixed wood	51	49	4
Sliding wood	57.1	62.8	−10

Table 4 Comparison of results for load case 2

Component	One-dimensional model S_1 (MPa)	Three-dimensional model S_3 (MPa)	Discrepancy $\frac{S_1-S_3}{S_1}$ (%)
Tank shell	372	338	9
Dome shell	490	493	−1
Tank longitudinal bulkhead	225	228	−1
Tank support rings	143	169	−18
Tank vacuum rings	278	267	4
Fixed wood	26	53.9	−107
Sliding wood	30.1	59.6	−98

Table 5 Comparison of results for load case 3

Component	One-dimensional model S_1 (MPa)	Three-dimensional model S_3 (MPa)	Discrepancy $\frac{S_1 - S_3}{S_1}$ (%)
Tank shell	357	323	10
Dome shell	492	490	0
Tank longitudinal bulkhead	244	210	14
Tank support rings	196	171	13
Tank vacuum rings	323	306	5
Fixed wood	39.1	42.7	−9
Sliding wood	45.1	70.3	−56

For static load case 1, the maximum stress of the sliding wood is slightly higher in the three-dimensional model (the discrepancy is 10%), and an agreement of maximum stress of the fixed wood is achieved. The three-dimensional model predicts lower maximum stress of the tank shell, the longitudinal bulkhead, and the support rings, in which the discrepancy are 7%, 20%, and 41%, respectively (see Table 3). This difference is mainly caused by the stress concentration at the connection between the spring elements and the tank shell elements in the one-dimensional model, whereas this stress concentration is prevented by simulating the reasonable contact surface between the tank and the wood in the three-dimensional model.

For dynamic load case 2, the maximum stresses of both fixed and sliding wood obtained by the three-dimensional model is twice larger than the results obtained using the one-dimensional model, which results in the larger stress of the tank support rings in the three-dimensional model (see Table 4). In addition, the discrepancies for the other tank structures between the two models are within 10%.

For dynamic load case 3, the one-dimensional model underestimates the maximum stress of both fixed and sliding wood, in which the discrepancy is −9% and −56%, respectively, although it slightly overestimates the maximum stress of the tank shell, the longitudinal bulkhead, and the support rings, in which the discrepancies are within 15% (see Table 5).

Figure 7 shows the comparisons of the results obtained by the two models for all load cases. It is seen that the one-dimensional model overestimates the maximum stress of the longitudinal bulkhead and the tank support rings for load cases 1 and 3, although it underestimates the maximum stress of the tank support rings for load case 2 (see Figs. 7A, B). This difference may be due to the acceleration angle equal to 0 in load case 2. It is found that the discrepancies for both longitudinal bulkhead and support rings increase with the increasing acceleration angle. From Fig. 7C, it is seen that the one-dimensional model slightly overestimates the maximum stress of the tank shell for all cases, and the discrepancies in all cases are close. Besides, there is little difference in the maximum stress of the dome shell and the tank vacuum rings between the two models for all load cases (see Figs. 7D, E). This is because that dome shell and tank vacuum rings are far away from the contact area, and consequently, the effect of the contact is little. Figures 7F, G shows that the discrepancies for both the fixed and sliding wood in load case 1 are smaller than those in load case 2 and case 3, which indicates that the effect of contact on the stress prediction for wood is more significant in the two dynamic load cases.

To sum up, a good agreement of the maximum stress of the dome shell and the tank vacuum rings between the two models is achieved. The results indicate that the contact between the tank and the wood has a significant effect on the predictions with respect to the stress of the longitudinal bulkhead, the support rings, and the wood for all load cases. Therefore, it is important to take the contact into account in a reasonable way for assessing the strength of the tank structures and the wood.

5.3.2. Comparison of stress distribution. The stress distributions of the sliding wood, the dome shell, and the tank shell obtained by both one-dimensional and three-dimensional models for load case 1 are shown in Figs. 8–10.

Figure 8 shows the comparison of stress distribution of the sliding wood. It is seen that half of the left wood in the one-dimensional model has been removed because of the detected tensile stress. A large stress occurs at the right end of the wood in both models. This is caused by the 30° of the acceleration angle in load case 1. From the result of the three-dimensional model, it is found that the stress distribution in both width and thickness directions of the wood is not uniform. However, the one-dimensional model is not able to simulate this phenomenon because of the limitations of the spring elements. Besides, the maximum stress obtained from the one-dimensional model is slightly lower than that obtained from the three-dimensional model.

From Fig. 9, it is observed that the maximum stress obtained from both models is located at the connection area of the dome and the tank. A good agreement of stress distribution of the dome shell between the two models is achieved, which indicates that the limitations of the spring elements have little effect on the stress distribution of the dome shell. This is because the distance between the dome and the wood is large. It is concluded that the one-dimensional model can predicate reasonable stress of the dome shell.

Figure 10 shows the stress distribution of the tank shell obtained from both models. The stresses obtained from the three-dimensional model are slightly lower than the results obtained from the one-dimensional model, especially the stresses at the contact area. This is because the three-dimensional model takes into account the contact surface between the tank shell and the wood and consequently reduces the stress concentration, whereas the contact force is acting on the nodes of spring elements in the one-dimensional model and the stress concentration is induced.

6. Conclusion

In this study, an innovative three-dimensional model has been proposed to assess the strength of the Type-C independent cargo tank structures, in which the nonlinear contact between the tank and the supporting wood is considered. Numerical simulations using nonlinear finite element software LS-DYNA have been carried out to test a 22,000-m^3 LPG carrier. Three load cases have been considered, including one static and two dynamic. Compared with the typical one-dimensional model which is on basis of the spring elements, the simulation results calculated by the three-dimensional model are summarized as follows:

1) A good agreement of the maximum stress of the dome shell and the tank vacuum rings between the two models is achieved for all load cases. However, because of the limitations of the spring elements, the one-dimensional

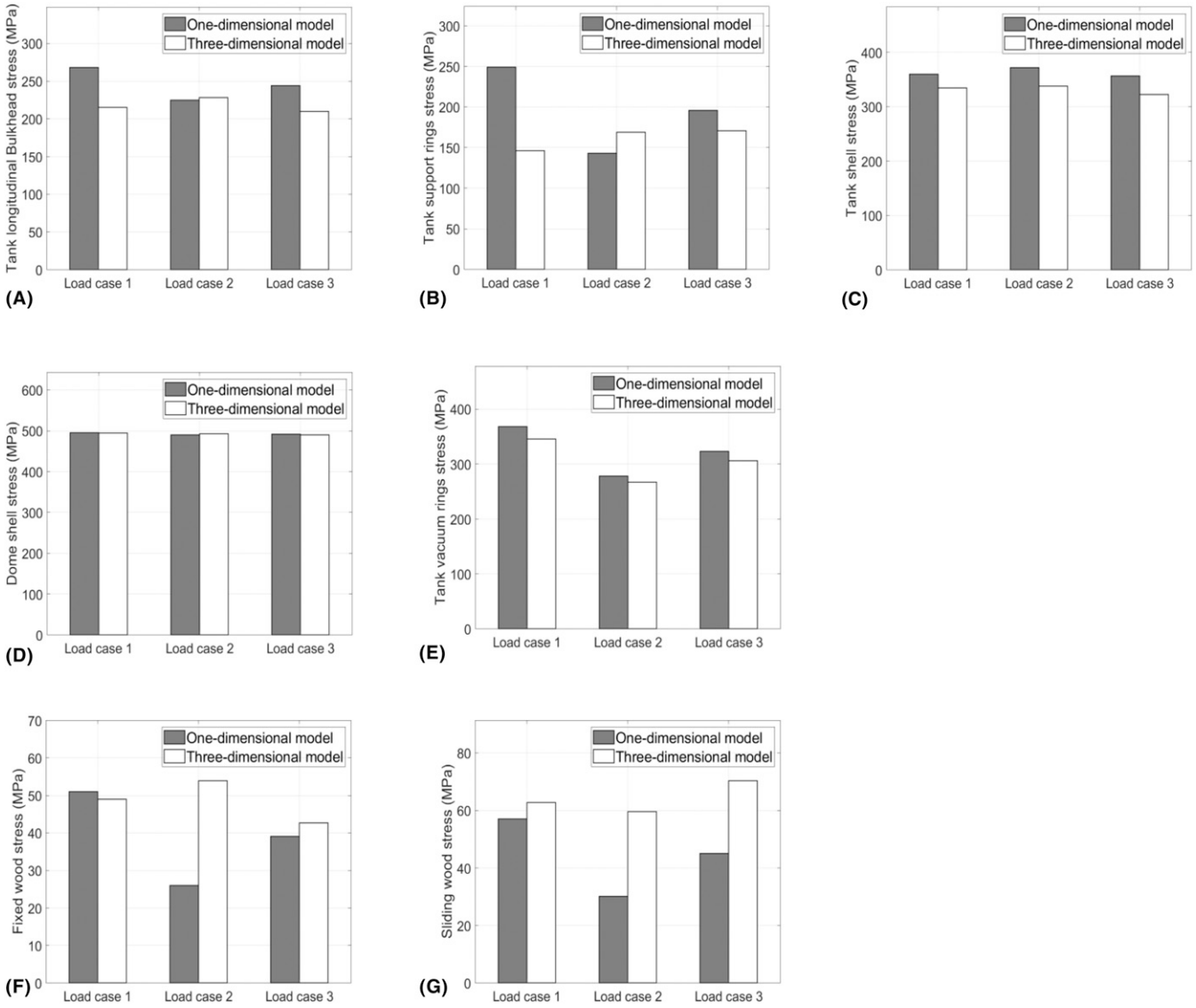

Fig. 7 Comparisons of the results obtained by the two models for the three load cases

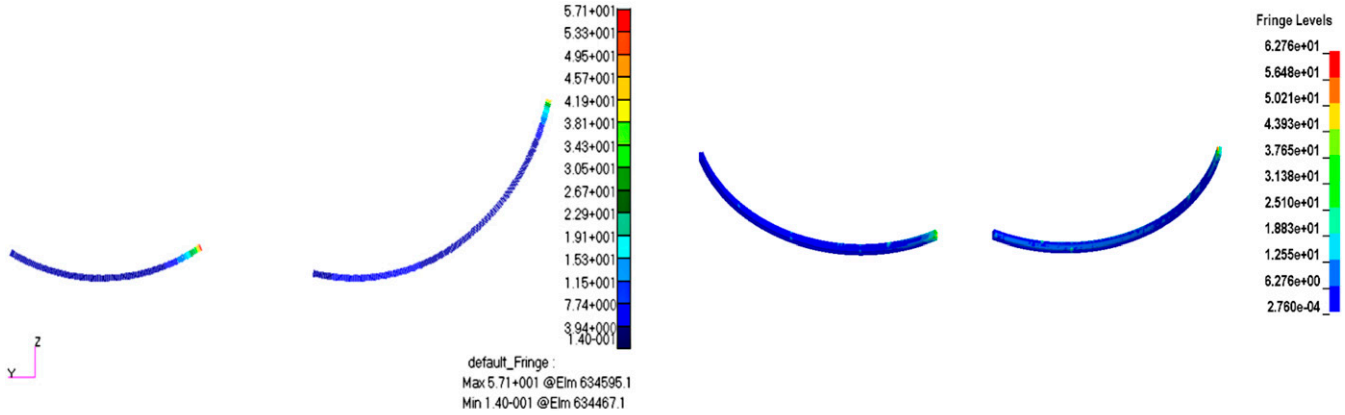

Fig. 8 Comparison of stress distribution of the sliding wood for load case 1

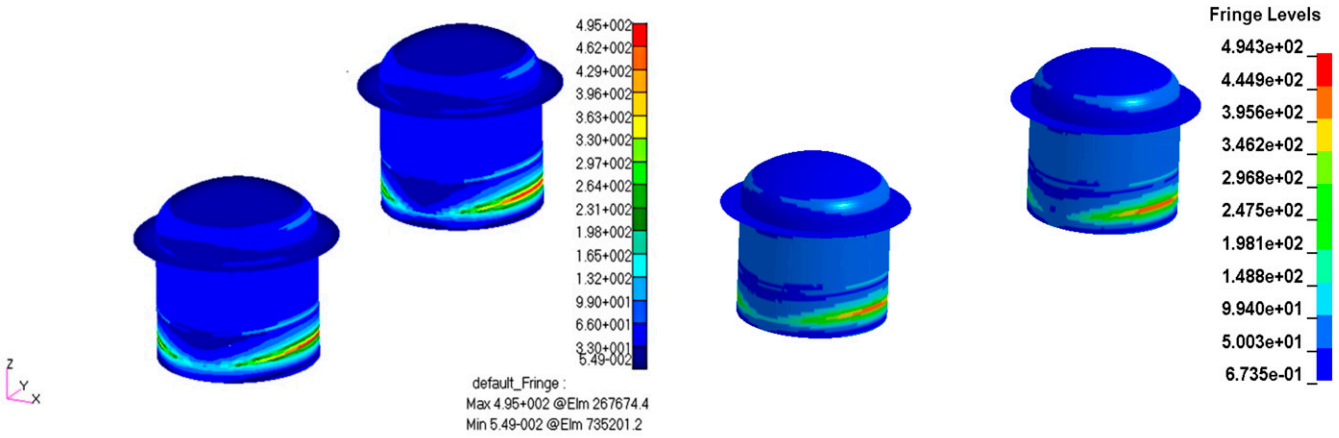

(A) Stress of the dome shell in one-dimensional model **(B)** Stress of the dome shell in three-dimensional model

Fig. 9 Comparison of stress distribution of the dome shell for load case 1

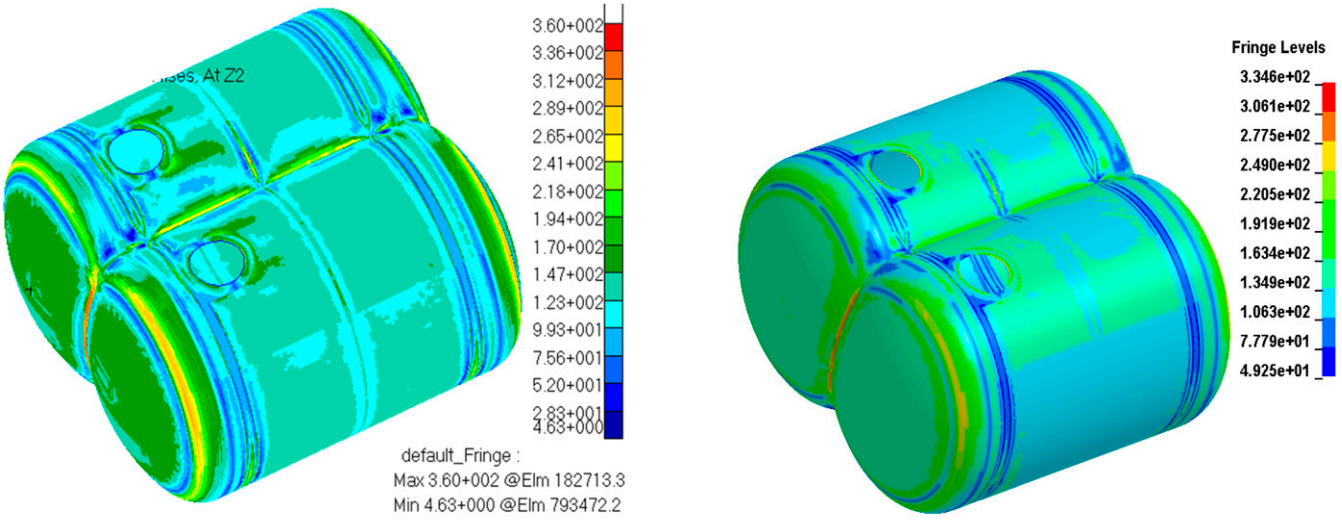

(A) Stress of the tank shell in one-dimensional model **(B)** Stress of the tank shell in three-dimensional model

Fig. 10 Comparison of stress distribution of the tank shell for load case 1

model overestimates the maximum stresses of the tank shell for all cases, and the longitudinal bulkhead and the support rings for load cases 1 and 3.

2) The one-dimensional model predicts lower maximum stresses of both fixed and sliding woods, especially for the two dynamic load cases (i.e., load cases 2 and 3), which indicates that it may be not conservative with respect to verifying the supporting wood stress.
3) The acceleration angle in the load case has a significant effect on the discrepancy of the predictions between the two models.
4) The three-dimensional model could provide more accurate predictions as it takes into account the nonlinear contact between the cargo tank and the wood in a more reasonable way. However, the cradles of the tank are regarded as rigid foundation with no deformation at the lower surface of the laminated wood. Further investigations are needed to consider this boundary effect.

References

American Bureau of Shipping (ABS) 2010 *Guide for Building and Classing Liquefied Gas Carriers with Independent Tanks*, Houston, TX: American Bureau of Shipping.

Blanc, H. M., Fleuren, H. A., and Krikke, H. R. 2004 Redesign of a recycling system for LPG-tanks, *OR Spectrum*, **26**(2), 283–304.

Bureau Veritas (BV) 2012 *ND371 Type C Tank Support Calculations*.

China Classification Society (CCS) 2016 *Rules for Construction and Equipment of Ships Carrying Liquefied Gases in Bulk*, Beijing, China: China Classification Society.

DET NORSKE VERITAS (DNV) 2013a *Strength Analysis of Independent Type C Tanks*, Oslo, Norway: DNV.

DET NORSKE VERITAS (DNV) 2013b *Strength Analysis of Liquefied Gas Carriers with Independent Type B Prismatic Tanks*, Oslo, Norway: DNV.

HALLQUIST, J. O. 2013 LS-DYNA user's manuals version 971, vol. 1 & 2. Livermore, CA: Livermore Software Technology Co.

INTERNATIONAL MARITIME ORGANIZATION (IMO) 2014 *International Code for the Construction and Equipment of Ships Carrying Liquefied Gases in Bulk: IGC Code*, London, United Kingdom: IMO.

LEE, J. H., KIM, Y. J., AND HWANG, S. 2015 Computational study of LNG evaporation and heat diffusion through a LNG cargo tank membrane, *Ocean Engineering*, **106**, 77–86.

LIM, W., CHOI, K., AND MOON, I. 2013 Current status and perspectives of liquefied natural gas (LNG) plant design, *Industrial & Engineering Chemistry Research*, **52**(9), 3065–3088.

LLOYD'S REGISTER 2016 *Primary Hull and Cargo Tank Supporting Structure of Type C Liquefied Gas Carries*, London, UK: Lloyd's Register.

MOROSUK, T., TSATSARONIS, G., BOYANO, A., AND GANTIVA, C. 2012 Advanced exergy-based analyses applied to a system including LNG regasification and electricity generation, *International Journal of Energy and Environmental Engineering*, **3**(1), 1.

REMELJEJ, C. W. AND HOADLEY, A. F. A. 2006 An exergy analysis of small-scale liquefied natural gas (LNG) liquefaction processes, *Energy*, **31**(12), 2005–2019.

SENJANOVIĆ, I., SENJANOVIĆ, T., LJUŠTINA, A. M., AND RUDAN, S. 2006 Structure design of cargo tanks in river liquefied gas carriers, *Proceedings*, DESIGN, May 15–18, Dubrovnik, Croatia.

THE WORLD LP GAS ASSOCIATION 2010 *Statistical Review of Global LP Gas*, Paris, France: WLPGA.

THIAGARAJAN, K. P. AND SEAH, R. 2016 *Liquefied Natural Gas Carriers*, Springer Handbook of Ocean Engineering, Springer, Cham: Springer Handbooks, pp. 963–984.